Mechanical Systems and Signal Processing 168 (2022) 108702

Contents lists available at ScienceDirect

Mechanical Systems and Signal Processing

journal homepage: www.elsevier.com/locate/ymssp

Absorption performance of nonplanar periodic structures solved by layered rigorous coupled-wave analysis

Yuzhen Yang [a], Han Jia [b,c,*], Hailin Cao [d], Xuecong Sun [a,b], Han Zhao [a,b], Yafeng Bi [a], Jun Yang [a,b,*]

[a] Key Laboratory of Noise and Vibration Research, Institute of Acoustics, Chinese Academy of Sciences, Beijing 100190, People's Republic of China
[b] University of Chinese Academy of Sciences, Beijing 100049, People's Republic of China
[c] State Key Laboratory of Acoustics, Institute of Acoustics, Chinese Academy of Sciences, Beijing 100190, People's Republic of China
[d] School of Materials Science and Engineering, Harbin Institute of Technology (Shenzhen), Shenzhen 518055, People's Republic of China

ARTICLE INFO

Communicated by Wieslaw Ostachowicz

Keywords:
Sound absorption performance
Porous material
Nonplanar periodic structure
Layered rigorous coupled-wave analysis
Wide frequency range

ABSTRACT

Porous materials with corrugated surfaces are widely used in the field of noise control, as they can effectively convert sound energy into heat resulting in sound absorption. It is important to predict the absorption coefficients of sound-absorbing devices for the design of appropriate shape and size. In this study, a semi-analytic method of layered rigorous coupled-wave analysis (LRCWA) is proposed to predict the absorption of nonplanar periodic materials. Starting from the division of corrugated surfaces into multiple layers, we process the sound behavior in each layer as in a rectangular periodic modulation structure. By connecting the interlayer boundary continuity conditions, the acoustic coupling equation of the whole structure can be established. The effectiveness and practicability of the LRCWA method is validated based on the comparisons with the experimental data and the simulation of finite element method. Besides the absorption coefficient that is mainly discussed in this work, the proposed method is universal in analyzing the physical properties of nonplanar periodic structures, which can greatly accelerate the delicate design and optimization of such structures.

1. Introduction

In practice, many corrugated structures made of porous material with wedge and semi-ellipse surfaces are installed on the wall for sound absorption [1–18]. Comparing to flat surfaces, structures with nonplanar surfaces achieve a gradual impedance that allows sound wave to enter absorbers smoothly, thus sound energy can be dissipated more fully in the porous material. Historically, widespread attention to acoustic wedges stemmed from searching the optimal geometry, dimensions and suitable material for building an anechoic chamber [1–8]. The researchers initially designed and optimized acoustic wedges by testing the absorption effect of different samples [1–3]. In 1946, Beranek and Sleeper [1] reported an important experimental study over five different types of structures, including linear wedge structures, exponential wedge structures and pyramid structures. The best structure of around 1000 different specimens was found to be wedge-like and manufactured from glass fibers. Analogous experiment was carried out by Koidan et al. [2] on a hybrid wedge composed of different weight materials and air space. However, it is a cumbersome and time-consuming task to optimize the design of acoustic wedges only through experimental measurements.

* Corresponding authors.
E-mail addresses: hjia@mail.ioa.ac.cn (H. Jia), jyang@mail.ioa.ac.cn (J. Yang).

https://doi.org/10.1016/j.ymssp.2021.108702
Received 19 July 2021; Received in revised form 24 October 2021; Accepted 26 November 2021
Available online 8 December 2021

With the improvement of numerical computing capabilities, theoretical solutions and numerical simulations for acoustic wedges have been greatly developed [4–6,9–17], which makes it possible to design suitable acoustic wedges before the manufacture and measurement of many different samples. Easwaran and Munjal [4] proposed a finite element method (FEM) based on the bulk reaction concept to predict the reflection characteristics of a wedge with normal incidence. The finite element (FE) model considered the wave propagation in the wedge material, and the theoretical predictions matched with the experimental results carried out by Koidan et al. in 1972 [2]. Similarly, Wang and Tang [5] made use of a boundary element method to model the behavior of sound normally incident on a wedge located in an impedance tube. In 2006, Kar and Munjal [13] proposed a boundary-condition-transfer algorithm for analyzing the performance of acoustic wedges. This method used the plane wave propagation and a wave coupling between the tapered wedge and the surrounding air cavity. In 2019, Zhao and coworkers [17] developed the finite-difference time-domain analysis for predicting sound absorption coefficients of acoustic wedges. The method was illustrated in a two-dimensional sound field, and the factors affecting absorption coefficients were discussed. Recently, Dario et al. improved the design of Biot-modeled foams [19] and applied a meta-core solution inside an acoustic package [20] to estimate acoustic performances of porous materials with embedded periodic inclusions. In most works, correct solutions are obtained by numerically calculating the local sound field point by point and matching the boundary conditions of different media. Such a process requires a lot of computing resources. Therefore, using these methods to optimize the shape and sizes of absorbers will be a complex and time-consuming task, because gradual changes of the configuration are required and a large number of iterative calculations are inevitable.

In this paper, we propose a novel semi-analytic method of layered rigorous coupled-wave analysis (LRCWA) to solve the sound performance of nonplanar periodic structures more easily. This method is based on the rigorous coupled-wave analysis (RCWA) method which was used for analyzing the diffraction of periodic acoustic gratings [21]. In the method of LRCWA, a corrugated material is divided into many thin layers so that each layer can be approximated as a rectangular periodic modulation. Therefore, the sound pressure of each layer can be processed the same as that of a single layer. Then, the interlayer coupling is determined by the boundary continuity condition between layers, and the fundamental governing equations of the whole structure is established to solve the reflection, transmission and sound absorption coefficients of the nonplanar periodic structure. In the method of LRCWA, evanescent modes are fully considered to ensure a high accuracy of the calculation results. In addition, the sound energy of each order can be obtained directly, which is helpful to understand the physical mechanism of sound propagation and regulate the acoustic characteristics of the structure.

The remainder of this paper is organized as follows. Section 2 explains the method of LRCWA and proposes an iterative solution algorithm to ensure the convergence and correctness of the numerical solution. Section 3 presents the method to extract the effective acoustic parameters of the porous material by testing the reflection coefficients of two planar structures in an impedance tube. Section 4 predicts the sound absorption coefficients of five samples with different shapes or sizes using the method of LRCWA. The results consistent with the measured absorption coefficients verify the correctness of the LRCWA method. In Section 5, the broadband sound absorption coefficients are predicted, and the effects of shape and geometric parameters on the sound absorption coefficient are discussed. Section 6 analyzes the effects of the shape and geometric parameters of large-scale structures on the sound absorption performance in low frequency range. By scanning geometric parameters or combining genetic algorithm, the geometric parameters of structures with different shapes are optimized to achieve a good sound absorption performance in a wide frequency range. Section 7 outlines the conclusions of this study.

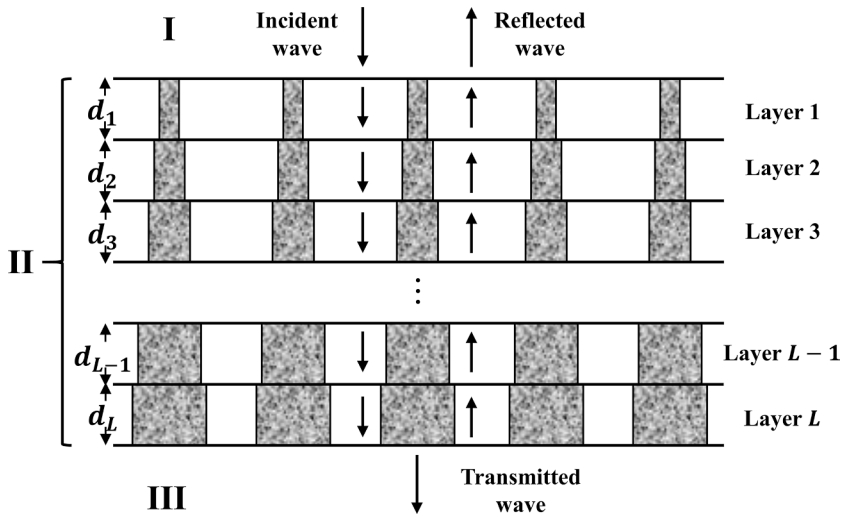

Fig. 1. Illustration of incident, reflected and transmitted sound waves in the layered rigorous coupled-wave analysis.

2. Method of LRCWA

2.1. Semi-analytic modeling and fundamental governing equations

Multi-layer composite materials and absorption materials with nonplanar surfaces are more usual than the single-layer flat material with a regular modulation. As shown in Fig. 1, a nonplanar structure can be recognized as the superposition of multiple single-layer periodic acoustic materials. The method of LRCWA for calculating and analyzing the absorption performance of the corrugated acoustic material is derived from the basis of the single-layer acoustic grating [21]. The sound field is divided into three areas, including the incident area I and transmitted area III with background air, and the area II within the periodic material that is divided into L layers because of the different modulation of each layer. The sound pressure in every area can be written as:

$$P_I = \exp(-jk_{x0}x - jk_{z0}z) + \sum_i R_i \exp(-jk_{xi}x + jk_{zi}z), \tag{1a}$$

$$P_l = \sum_i S_{li}(z)\exp(-jk_{xi}x), \quad (l = 1, 2, \cdots, L-1, L), \tag{1b}$$

$$P_{III} = \sum_i T_i \exp[-jk_{xi}x - jk_{zi}(z-D)], \tag{1c}$$

where $k_{x0} = k_0\sin\theta$, $k_{z0} = k_0\cos\theta$ and $k_{xi} = k_0\sin\theta + iK(K = 2\pi/T, i = -\infty, \cdots, 0, +\infty)$. For $k_{xi} < k_0$, there is $k_{zi} = \sqrt{k_0^2 - k_{xi}^2}$; for $k_{xi} > k_0$, there is $k_{zi} = -j\sqrt{k_{xi}^2 - k_0^2}$. Here k_0 is the wave vector in air; k_{xi} and k_{zi} are the wave vectors in x and z directions, respectively. θ is the incident angle; T and D are the period and thickness of the whole structure, respectively; R_i and T_i are normalized amplitudes of the reflected wave and transmitted wave, respectively; S_{li} is the ith coefficient of the pressure within the Layer l. In one-dimensional periodic acoustic structure, the acoustic wave equation in inhomogeneous medium is

$$\nabla^2 P + k_0^2 n^2(x) P - \frac{\partial \ln\rho(x)}{\partial x}\frac{\partial P}{\partial x} = 0. \tag{2}$$

The coefficients related to the refractive index and mass density are expanded into the corresponding series as:

$$n_l^2(x) = \sum_m x_m^l \exp(-jmKx), \tag{3a}$$

$$\ln\rho_l(\mathrm{x}) = \sum_m y_m^l \exp(-jmKx). \tag{3b}$$

Substituting Eqs. (1b), (3a) and (3b) into Eq. (2), the coupled equations can be written as:

$$S_{li}^{''}(z) - k_{xi}^2 S_{li}(z) + k_0^2 \sum_j x_{i-j}^l S_{lj}(z) + \sum_k (i-k) K k_{xk} y_{i-k}^l S_{lk}(z) = 0. \tag{4}$$

Resemble all the coefficients $S_{li}(z)$ of modes into a vector, thus we can write $[\mathbf{S}_l^{''}] = [\mathbf{A}_l][\mathbf{S}_l]$. The matrix $\mathbf{A}_l = \mathbf{K}_x^2 - k_0^2\mathbf{X}_l - K\mathbf{K}_x\mathbf{Y}_l$ is the coefficient matrix of the coupled differential equation; the elements of $\mathbf{X}_l$ and $\mathbf{Y}_l$ are $X_{m,n}^l = x_{m-n}^l$ and $Y_{m,n}^l = (m-n)y_{m-n}^l$, respectively; and the elements of the diagonal matrix $\mathbf{K}_x$ are $K_{i,i} = k_{xi}$. The solution can be written in the form as:

$$S_{li}(z) = \sum_m w_{i,m}^l \left\{ c_m^{l+}\exp\left(-q_m^l z\right) + c_m^{l-}\exp\left[q_m^l(z-d_1)\right] \right\}, \quad (l = 1), \tag{5a}$$

$$S_{li}(z) = \sum_m w_{i,m}^l \left\{ c_m^{l+}\exp\left[-q_m^l\left(z - \sum_{p=1}^{l-1} d_p\right)\right] + c_m^{l-}\exp\left[q_m^l\left(z - \sum_{p=1}^{l} d_p\right)\right] \right\}, \quad (l = 2, 3, \cdots, L), \tag{5b}$$

where q_m^l is the square root of the eigenvalue and $w_{i,m}^l$ is the corresponding eigenvector of matrix $\mathbf{A}_l$. The coefficients c_m^{l+} and c_m^{l-} can be determined by the continuity conditions of interlayer boundaries. The normal particle vibration velocity is $v_z = (-1/j\omega\rho)\cdot(\partial \mathrm{P}/\partial \mathrm{z})$ for simple harmonic wave. By expanding the reciprocal of the normalized mass density as $\rho_0/\rho_l(x) = \sum_m z_m^l \exp(-jmKx)$, the particle vibration velocity can be expressed as:

$$v_{li}^z = -\frac{1}{j\omega\rho_0}\sum_q z_{(i-q)}^l \sum_m w_{q,m}^l \left\{ -q_m^l c_m^{l+}\exp\left(-q_m^l z\right) + q_m^l c_m^{l-}\exp\left[q_m^l(z-d_1)\right] \right\}, \quad (l = 1), \tag{6a}$$

$$v_{li}^{z}=-\frac{1}{j\omega\rho_0}\sum_{q}z_{(i-q)}^{l}\sum_{m}w_{q,m}^{l}\left\{-q_m^l c_m^{l+}\exp\left[-q_m^l\left(z-\sum_{p=1}^{l-1}d_p\right)\right]+q_m^l c_m^{l-}\exp\left[q_m^l\left(z-\sum_{p=1}^{l}d_p\right)\right]\right\},\quad(l=2,3,\cdots,L). \tag{6b}$$

Thus, the continuity condition at the first interface can be written as:

$$\begin{bmatrix}\Delta_{i0}\\ jk_0cos\theta\Delta_{i0}\end{bmatrix}+\begin{bmatrix}\mathbf{I}\\ -j\mathbf{K}_z\end{bmatrix}[\mathbf{R}]=\begin{bmatrix}\mathbf{W}_1 & \mathbf{W}_1\mathbf{E}_1\\ \mathbf{V}_1 & -\mathbf{V}_1\mathbf{E}_1\end{bmatrix}\begin{bmatrix}\mathbf{C}_1^{+}\\ \mathbf{C}_1^{-}\end{bmatrix}. \tag{7}$$

For the intermediate layers, there are

$$\begin{bmatrix}\mathbf{W}_l & \mathbf{W}_l\mathbf{E}_l\\ \mathbf{V}_l & -\mathbf{V}_l\mathbf{E}_l\end{bmatrix}\begin{bmatrix}\mathbf{C}_l^{+}\\ \mathbf{C}_l^{-}\end{bmatrix}=\begin{bmatrix}\mathbf{W}_{l-1}\mathbf{E}_{l-1} & \mathbf{W}_{l-1}\\ \mathbf{V}_{l-1}\mathbf{E}_{l-1} & -\mathbf{V}_{l-1}\end{bmatrix}\begin{bmatrix}\mathbf{C}_{l-1}^{+}\\ \mathbf{C}_{l-1}^{-}\end{bmatrix}. \tag{8}$$

At the last interface, the continuity condition is

$$\begin{bmatrix}\mathbf{W}_L\mathbf{E}_L & \mathbf{W}_L\\ \mathbf{V}_L\mathbf{E}_L & -\mathbf{V}_L\end{bmatrix}\begin{bmatrix}\mathbf{C}_L^{+}\\ \mathbf{C}_L^{-}\end{bmatrix}=\begin{bmatrix}\mathbf{I}\\ j\mathbf{K}_z\end{bmatrix}[\mathbf{T}]. \tag{9}$$

where $\mathbf{R}$, $\mathbf{T}$, $\mathbf{C}_l^{+}$ and $\mathbf{C}_l^{-}$ are the vectors of coefficients R_i , T_i , c_m^{l+} and c_m^{l-} , respectively; $\mathbf{W}_l$ is the matrix of eigenvector $w_{i,m}^{l}$; $\mathbf{I}$ is the identity matrix; Δ_{i0} is a vector in which the element corresponding to zero-order equals to 1 and others are zero; for simplicity, set a matrix $\mathbf{V}_l$ as $\mathbf{V}_l=\mathbf{Z}_l\mathbf{W}_l\mathbf{Q}_l$; the elements of matrix $\mathbf{Z}_l$ are $Z_{m,n}^{l}=z_{m-n}^{l}$; the elements of diagonal matrixes $\mathbf{Q}_l$, $\mathbf{E}_l$ and $\mathbf{K}_z$ are q_m^l , $\exp(-q_m^l d_l)$ and k_{zi} , respectively.

Thus, the following equation can be obtained by matrix calculation,

$$\begin{bmatrix}\Delta_{i0}\\ jk_0cos\theta\Delta_{i0}\end{bmatrix}+\begin{bmatrix}\mathbf{I}\\ -j\mathbf{K}_z\end{bmatrix}[\mathbf{R}]=\left\{\prod_{l=1}^{L}\begin{bmatrix}\mathbf{W}_l & \mathbf{W}_l\mathbf{E}_l\\ \mathbf{V}_l & -\mathbf{V}_l\mathbf{E}_l\end{bmatrix}\begin{bmatrix}\mathbf{W}_l\mathbf{E}_l & \mathbf{W}_l\\ \mathbf{V}_l\mathbf{E}_l & -\mathbf{V}_l\end{bmatrix}^{-1}\right\}\begin{bmatrix}\mathbf{I}\\ j\mathbf{K}_z\end{bmatrix}[\mathbf{T}]. \tag{10}$$

According to Eq. (10), the solution of the coefficient matrixes is uniquely definite for a certain acoustic structure and incidence condition. It means that the vectors of reflected coefficients $\mathbf{R}$ and transmitted coefficients $\mathbf{T}$ can be solved by Eq. (10) theoretically. The total reflection coefficient is $R_I=\sum R_iR_i^{*}\mathrm{Re}(k_{zi}/k_{z0})$ and the total transmission coefficient is $T_I=\sum T_iT_i^{*}\mathrm{Re}(k_{zi}/k_{z0})$, so the absorption coefficient is $\alpha=1-R_I-T_I$.

2.2. Iterative solution method

A direct solution of Eq. (10) involves several matrix inversion operations, which will cause significate and even intolerable errors in the final result. Referring to the similarity algorithm in optical structure [22–27], the non-convergence of algorithm can be avoided by an iterative solution, and the specific operation steps are given below.

The last four items on the right side of Eq. (10) can be written as:

$$\begin{bmatrix}\mathbf{W}_L & \mathbf{W}_L\mathbf{E}_L\\ \mathbf{V}_L & -\mathbf{V}_L\mathbf{E}_L\end{bmatrix}\begin{bmatrix}\mathbf{W}_L\mathbf{E}_L & \mathbf{W}_L\\ \mathbf{V}_L\mathbf{E}_L & -\mathbf{V}_L\end{bmatrix}^{-1}\begin{bmatrix}\mathbf{I}\\ j\mathbf{K}_z\end{bmatrix}[\mathbf{T}]=\begin{bmatrix}\mathbf{W}_L & \mathbf{W}_L\mathbf{E}_L\\ \mathbf{V}_L & -\mathbf{V}_L\mathbf{E}_L\end{bmatrix}\begin{bmatrix}\mathbf{E}_L & 0\\ 0 & \mathbf{I}\end{bmatrix}^{-1}\begin{bmatrix}\mathbf{W}_L & \mathbf{W}_L\\ \mathbf{V}_L & -\mathbf{V}_L\end{bmatrix}^{-1}\begin{bmatrix}\mathbf{f}_{L+1}\\ \mathbf{g}_{L+1}\end{bmatrix}[\mathbf{T}], \tag{11}$$

where the iterative matrix $\mathbf{f}_{L+1}$ and $\mathbf{g}_{L+1}$ are $\mathbf{f}_{L+1}=\mathbf{I}$ and $\mathbf{g}_{L+1}=j\mathbf{K}_z$, respectively. Introduce new iterative matrixes as:

$$\begin{bmatrix}\mathbf{a}_L\\ \mathbf{b}_L\end{bmatrix}=\begin{bmatrix}\mathbf{W}_L & \mathbf{W}_L\\ \mathbf{V}_L & -\mathbf{V}_L\end{bmatrix}^{-1}\begin{bmatrix}\mathbf{f}_{L+1}\\ \mathbf{g}_{L+1}\end{bmatrix}, \tag{12}$$

and there is $\mathbf{T}=\mathbf{a}_L^{-1}\mathbf{E}_L\mathbf{T}_L$. Through further arrangement and calculation, following equation can be obtained:

$$\begin{bmatrix}\mathbf{f}_L\\ \mathbf{g}_L\end{bmatrix}[\mathbf{T}_L]=\begin{bmatrix}\mathbf{W}_L & \mathbf{W}_L\mathbf{E}_L\\ \mathbf{V}_L & -\mathbf{V}_L\mathbf{E}_L\end{bmatrix}\begin{bmatrix}\mathbf{I}\\ \mathbf{b}_L\mathbf{a}_L^{-1}\mathbf{E}_L\end{bmatrix}[\mathbf{T}_L]=\begin{bmatrix}\mathbf{W}_L\left(\mathbf{I}+\mathbf{E}_L\mathbf{b}_L\mathbf{a}_L^{-1}\mathbf{E}_L\right)\\ \mathbf{V}_L\left(\mathbf{I}-\mathbf{E}_L\mathbf{b}_L\mathbf{a}_L^{-1}\mathbf{E}_L\right)\end{bmatrix}[\mathbf{T}_L]. \tag{13}$$

Therefore, the iterative matrixes are $\mathbf{f}_L=\mathbf{W}_L\left(\mathbf{I}+\mathbf{E}_L\mathbf{b}_L\mathbf{a}_L^{-1}\mathbf{E}_L\right)$ and $\mathbf{g}_L=\mathbf{V}_L\left(\mathbf{I}-\mathbf{E}_L\mathbf{b}_L\mathbf{a}_L^{-1}\mathbf{E}_L\right)$. Then, repeat the process for each layer to get the following equation:

$$\begin{bmatrix}\Delta_{i0}\\ jk_0cos\theta\Delta_{i0}\end{bmatrix}+\begin{bmatrix}\mathbf{I}\\ -j\mathbf{K}_z\end{bmatrix}[\mathbf{R}]=\begin{bmatrix}\mathbf{f}_1\\ \mathbf{g}_1\end{bmatrix}[\mathbf{T}_1]. \tag{14}$$

The coefficient vectors $\mathbf{R}$ and $\mathbf{T}_1$ can be solved by Eq. (14), and there is $\mathbf{T}=\mathbf{a}_L^{-1}\mathbf{E}_L\cdots\mathbf{a}_l^{-1}\mathbf{E}_l\cdots\mathbf{a}_1^{-1}\mathbf{E}_1\mathbf{T}_1$.

Next, we give a calculation example to illustrate the advantage of the iterative solution method. Without loss of generality, we

randomly selected a flat periodic structure with binary equal-proportional rectangular modulation. The corresponding parameters are set as follows: the modulation period is $T = 2\lambda$; the thickness of structure is $d = 3\lambda$; the refractive indices for two media are $n_1 = 1$ and $n_2 = 1.5$, respectively; the mass densities are $\rho_1 = \rho_2 = \rho_0$; and the incident angle θ equals to Bragg incident angle $\theta = \arcsin(\pi/(k_0 T))$.

In our previous work, it has been verified that such a flat periodic structure can be solved accurately by the method of RCWA [21]. To verify the superiority of the iterative algorithm, the convergence of diffraction efficiencies is firstly calculated by RCWA as a single-layer periodic material, whose results are shown as the solid lines in Fig. 2(a) and (b). Besides, the structure can be artificially divided into multiple layers. After the structure is divided into five layers with equal thickness, we adopt the direct solution and iterative algorithm of LRCWA to calculate the convergence of diffraction efficiencies, respectively. The results are shown as symbols in Fig. 2(a) and (b). Compared with the result of RCWA, direct solution generates huge and unacceptable errors while the result of iterative algorithm shows good and consistent convergence.

3. Effective acoustic parameters extraction

In the methods of LRCWA and RCWA, an important part is extracting the effective acoustic parameters of porous materials. Obtaining the accurate velocity and mass density that are required for calculation is indispensable to ensure a reliable calculation result. Here, we introduce an easy and convenient method to extract the effective acoustic parameters of porous materials by experimental measurement in the two-microphone impedance tube system [11].

Given the complex wave propagation constant γ and nondimensionalized acoustic impedance Z_m , there are complex effective sound velocity $c_m = \omega/(-j\gamma)$ and complex effective mass density $\rho_m = (-j\gamma\rho_0 c_0 Z_m)/\omega$. When a flat piece of porous material with thickness t backed with rigid wall is considered, the specific impedance is $\zeta = Z_m \coth(\gamma t)$. The reflection coefficient R and the specific impedance ζ satisfy the following equation:

$$\zeta = \frac{1+R}{1-R}. \tag{15}$$

For two pieces of porous material with different thicknesses t_1 and t_2 , there are

$$\zeta_1 = Z_m \coth(\gamma t_1), \tag{16a}$$

$$\zeta_2 = Z_m \coth(\gamma t_2). \tag{16b}$$

The nondimensionalized acoustic impedance Z_m is unique for a certain material, so we can obtain the equation $\zeta_1 \tanh(\gamma t_1) - \zeta_2 \tanh(\gamma t_2) = 0$ by eliminating Z_m in Eqs. (16a) and (16b). After obtaining the specific impedance ζ_1 and ζ_2 by measuring the reflection coefficients, the complex wave propagation constant γ can be solved numerically. Then, the acoustic impedance Z_m , effective sound velocity c_m and effective mass density ρ_m are all obtained.

In this study, the porous material we selected is a commonly used high-density sound-absorbing sponge. For obtaining the effective acoustic parameters, two pieces of sound absorbing sponge with thicknesses of 2 cm and 4.8 cm are measured in a two-microphone square impedance tube. The complex reflections are presented in Fig. 3. The real and imaginary reflection coefficients vary with the frequency. Two specific impedances ζ_1 and ζ_2 can be derived from Eq. (15). Then, the complex wave propagation constant γ, acoustic impedance Z_m , effective sound velocity c_m and effective mass density ρ_m can be obtained by numerical calculation. The results of the effective sound velocity and mass density are presented in Fig. 4. Both acoustic parameters are complex due to sound absorption. These effective acoustic parameters will be used later in the LRCWA method to calculate the absorption coefficients of different nonplanar structures of the absorbing sponge.

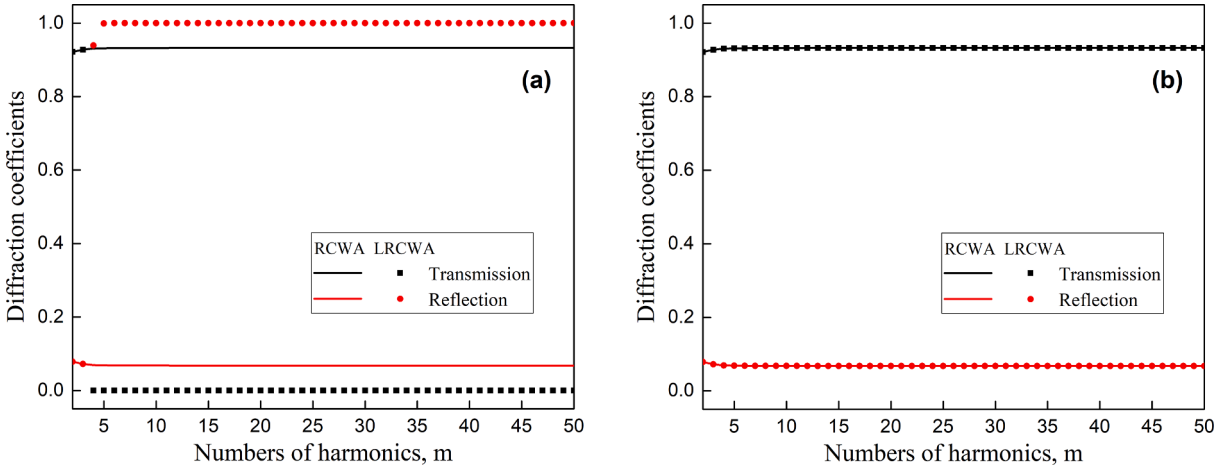

Fig. 2. Convergence of diffraction efficiencies dependence on the number of harmonics for (a) direct solution and (b) iterative solution.

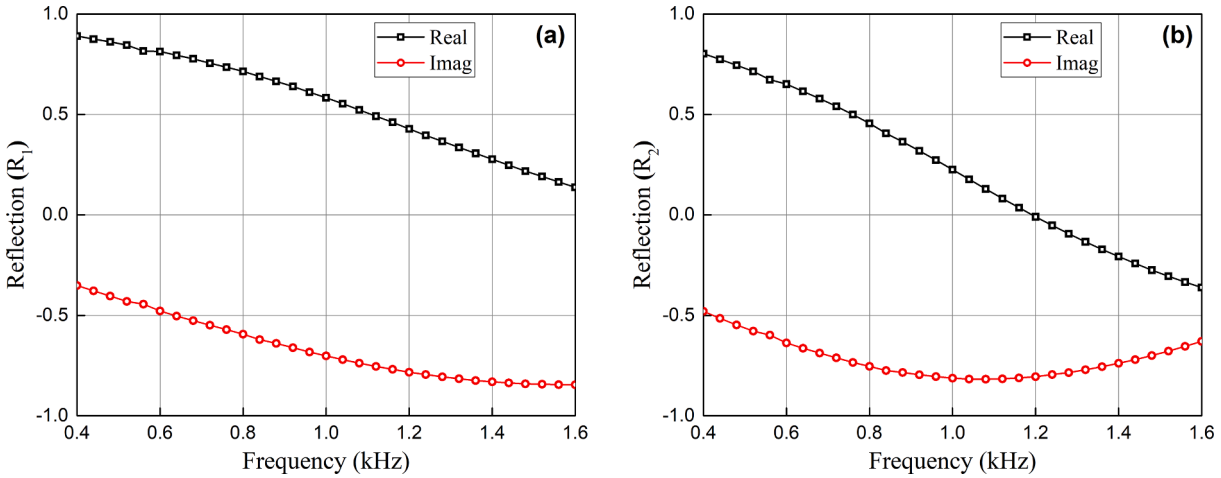

Fig. 3. Real and imaginary parts of the measured reflection coefficients of the flat absorbing sponges with (a) thickness $t_1 = 2$cm and (b) thickness $t_2 = 4.8$cm in the frequency range from 400 Hz to 1600 Hz.

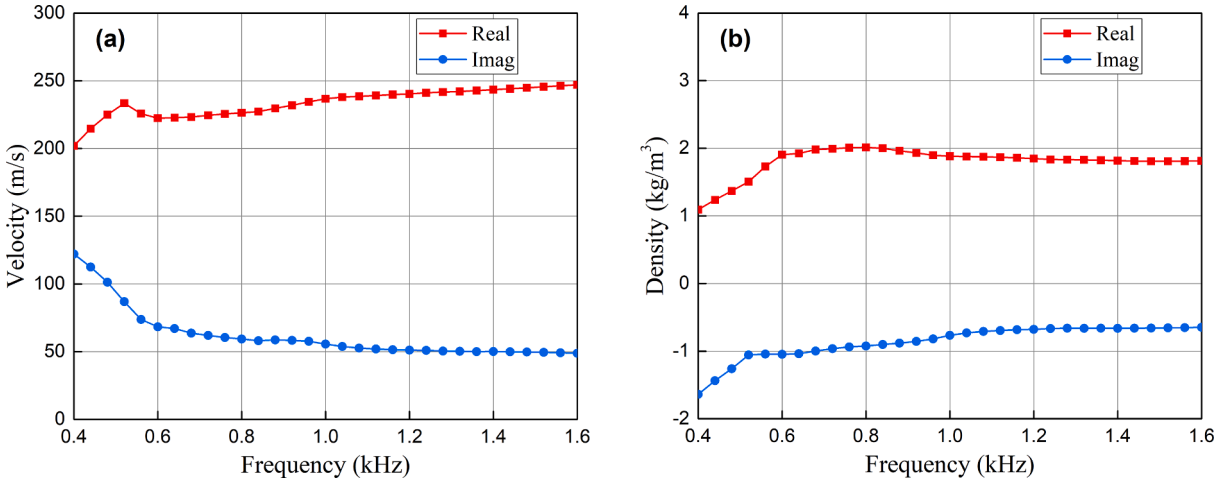

Fig. 4. Real and imaginary parts of (a) the effective sound velocity and (b) the effective mass density of the absorbing sponge in the frequency range from 400 Hz to 1600 Hz.

3. Experimental validation

In this part, we attempt to validate the semi-analytic method of LRCWA for nonplanar periodic acoustic material experimentally. To this end, we calculated and measured some specimens of sound-absorbing sponges with common nonplanar surfaces, including surfaces of plane, triangle, rectangle and T shape, as shown in Fig. 5. The geometric parameters of different structures are listed in Table 1, in which the samples with triangle surface have two sets of geometric parameters.

In the layering process of calculation, the surfaces of rectangle and T shape are simply divided into two layers and three layers according to different proportions, respectively. And the surface of triangle is divided into multiple layers to ensure that each layer is close to a rectangular periodic modulation. The effective acoustic parameters of the sound-absorbing sponge obtained from experiment (as shown in Fig. 4) are taken into the calculation of the absorption coefficients of the samples with nonplanar periodic surfaces. The predicted absorption coefficients with the LRCWA method are shown as the curves in Fig. 6(a).

In order to verify the accuracy and availability of the LRCWA method, above structures with surfaces of plane, triangle, rectangle and T shape are cut into square blocks with side length of 10 cm and tested in a square impedance tube. The measured absorption coefficients shown as symbols in Fig. 6(a) are very close to the calculation results of the proposed semi-analytic method. The prediction errors of the sound absorption coefficients with the LRCWA method were examined over the entire measured frequency range. The prediction error rate was calculated by $|\alpha_m - \alpha_p|/\alpha_m$, where α_m is the measured absorption coefficient and α_p is the predicted absorption coefficient using the LRCWA method. The comparative results are shown as the solid curves in Fig. 6(b). All the mean values of the prediction errors are less than 10% as shown in Fig. 6(c). In other words, the highly consistent results verify the effectiveness and

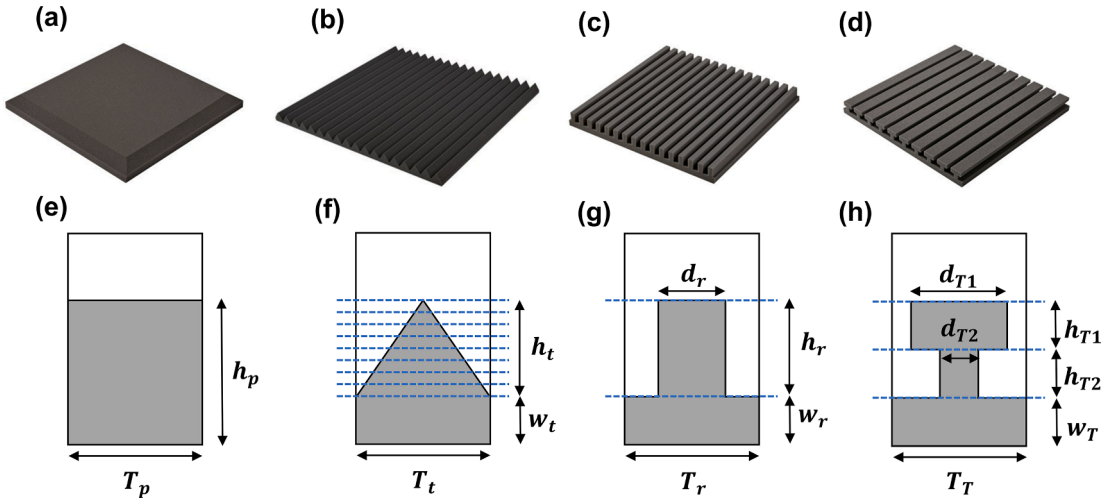

Fig. 5. Photos of the sound-absorbing sponges with surfaces of (a) plane, (b) triangle, (c) rectangle and (d) T shape. Cross sections of the sound-absorbing sponges with surfaces of (e) plane, (f) triangle, (g) rectangle and (h) T shape.

Table 1
The specific sizes of different shapes.

Shape	Size
Plane	$h_p = 48mm$
Triangle I	$T_{t1} = 25mm$, $w_{t1} = 9mm$, $h_{t1} = 16mm$
Triangle II	$T_{t2} = 50mm$, $w_{t2} = 10mm$, $h_{t2} = 37mm$
Rectangle	$T_r = 33mm$, $w_r = 19mm$, $h_r = 28mm$, $d_r = 15mm$
T shape	$T_T = 50mm$, $w_T = 19mm$, $h_{T1} = 15mm$, $h_{T2} = 15mm$, $d_{T1} = 14mm$, $d_{T2} = 35mm$

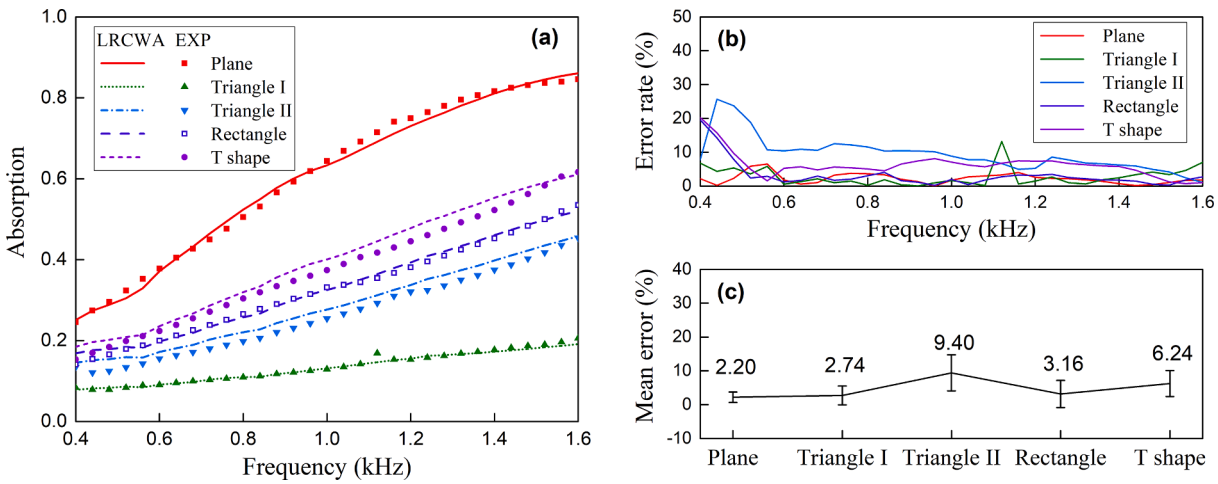

Fig. 6. (a) The sound absorption coefficients predicted using LRCWA (curves) and measured experimentally (symbols) of the absorbing sponge with different surfaces. (b) Percentage errors and (c) mean errors of the predicted absorption coefficients compared to the experimental results.

applicability of the LRCWA method in predicting the absorption coefficients of the nonplanar periodic acoustic materials.

4. Broadband adaptability

Since the accuracy and effectiveness of the LRCWA method have been verified, we apply the semi-analytic method to discuss the influences of the shape and size of the nonplanar periodic structures on the broadband sound absorption coefficient. Due to the limited

size of the impedance tube, the sizes of tested samples and the measurable frequency range are severely limited. However, the calculation and analysis of sound absorption using LRCWA will not be restricted as long as the effective acoustic parameters of the porous materials are given.

In this part, we mainly discuss the broadband absorption coefficients of nonplanar periodic sound-absorbing sponges, including the sponges with surfaces of plane, triangle, rectangle and ellipse as shown in Fig. 7. A geometric proportion parameter h/w representing the thickness ratio between the tip and the base is defined for the later discussion.

For obtaining the effective acoustic parameters in high frequency range, the flat sponges with thickness of 2 cm and 4.8 cm are cut into smaller cylindric samples with diameter of 29 mm and are tested in a small tube of Brüel&Kjær impedance tube Type 4206. The extracted effective acoustic parameters of the absorbing sponge in the frequency range from 400 Hz to 4800 Hz are shown in Fig. 8. Because the absorbing sponge is easily deformed and the size error influences the test results, the effective acoustic parameters in the low frequency range are slightly discrepant with the results tested in the square impedance tube. For the continuity of the effective acoustic parameters, the effective acoustic parameters tested in the small tube are selected for the calculation in the wide frequency range.

As mentioned above, the measurable frequency range of experiments are limited by the size of the impedance tube. Here, the simulation of FEM is selected as a comparison to the semi-analytic calculation of LRCWA. The configuration of the FE model is totally the same as that in the method of LRCWA, and the tested effective acoustic parameters are taken into the simulation of FEM.

In the first case, set the period as 5.5 cm and the overall thickness as $5\mathrm{cm}$, that is, $h+w=5\mathrm{cm}$. With a same geometry ratio $h/w=3/2$, the absorption coefficients for different surface shapes are presented in Fig. 9(a). The curves are the calculation results using LRCWA, and symbols are the simulation results using FEM. The results of two methods are in perfect agreement, which strongly proves the validity of the LRCWA method in the wide frequency range. For a same geometry ratio h/w , the total volume of the planar sponge is the largest, followed by the ellipse, and the triangle and rectangle are the same and the smallest. The absorption coefficient increases obviously with the increase of the volume of the absorbing sponge, especially in the low frequency range. Because of the same volume, the absorption coefficients of the sponges with surfaces of triangle and rectangle are the same in low frequency range. However, absorption coefficients appear different oscillations due to different surface shapes in high frequency range.

In the second case, in order to focus on the influence of the surface shapes, we constrain the total volume of the sponge to be constant to eliminate the effect of total volume. The thickness of the base remains the same and the sizes of the tips are adjusted to meet the volume limitation. The absorption coefficients for different surface shapes with the same volume of sponge are presented in Fig. 9 (b). The absorption coefficients below 1.2 kHz are almost not affected by the surface shapes. Only in high frequency range, the absorption coefficients will change significantly due to different surface shapes. The reason is that shape variations at a small scale make no difference to sound waves with large wavelength. The sizes of the above discussed structures are very small compared to the wave length below 1.2 kHz, so it is mainly the material volume rather than the shape that affects the low frequency absorption coefficient. Although the sound absorption coefficients shown in Fig. 9(b) are almost the same around 2.9 kHz, for a structure of the same volume but with a more unusual surface shape, a large change can occur in the absorption coefficient near 2.9 kHz.

Cases of varying the geometric ratio h/w while keep the overall thickness as $5cm$ are discussed as supplementary. The corresponding absorption coefficients of sponges with different surface shapes are shown in Fig. 10. Besides the results of different geometry ratios 4:1, 3:2 and 2:3, the absorption coefficient of plan sponge is also presented as a reference. For nonplanar sponges with surfaces of triangle, rectangle and ellipse, the increase of geometry ratio causes the reduction of the volume of sponge. As a result, the absorption coefficients decrease with the increase of geometry ratio, which is consistent with the aforementioned rule that higher quantity of the volume implies a better acoustic absorption.

5. Design and optimization of low frequency sound absorber

5.1. *Effective acoustic parameters in low frequency range*

High absorption in low frequency range is very important in sound absorber design, so it is necessary to increase the sizes of sound absorption structures and discuss the sound absorption performance in lower frequency range. Limited by the sizes of the impedance tube, the effective acoustic parameters of the porous material are extracted using the Johnson-Champoux-Allard (JCA) porous model

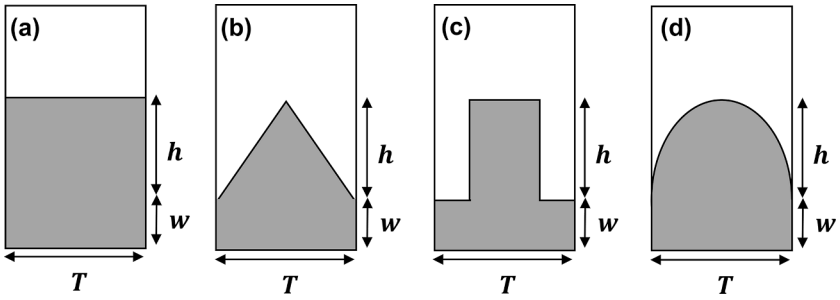

Fig. 7. Absorbing sponge with different surfaces of (a) plane, (b) triangle, (c) rectangle and (d) ellipse.

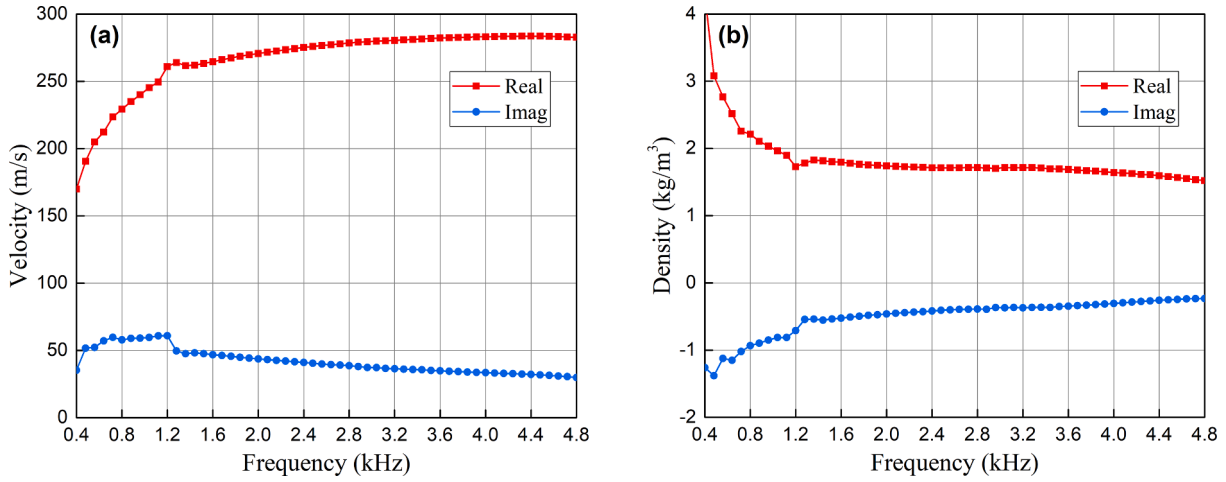

Fig. 8. Real and imaginary parts of (a) the effective sound velocity and (b) the effective mass density of the absorbing sponge in the frequency range from 400 Hz to 4800 Hz.

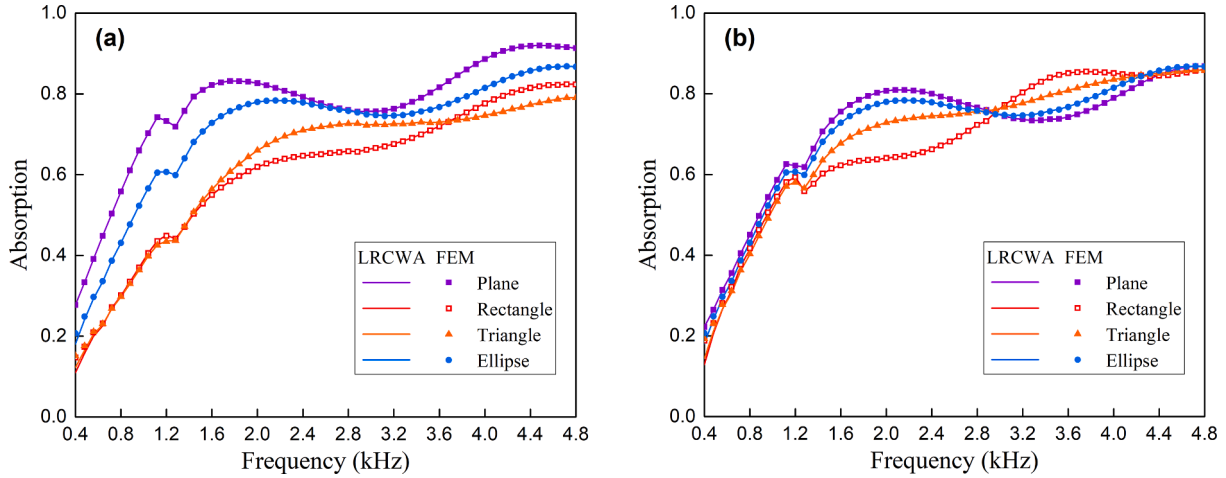

Fig. 9. Variations of absorption coefficients versus frequency for different surface shapes with (a) the same h/w ratio, (b) the same volume.

[28] and the required parameters are obtained directly from the research results of Doutres et al. in 2011 [29]. According to the JCA model, the effective mass density ρ_e and bulk modulus B_e can be expressed as:

$$\rho_e = \frac{\alpha_\infty \rho_0}{\phi}\left(1 + \frac{\sigma\phi}{j\omega\rho_0\alpha_\infty}\sqrt{1 + \frac{4j\alpha_\infty^2\eta\rho_0\omega}{\sigma^2\Lambda^2\phi^2}}\right), \tag{17a}$$

$$B_e = \frac{\gamma P_0}{\phi}\left[\gamma - (\gamma-1)\left(1 + \frac{8\eta}{j\Lambda'^2 N_p\omega\rho_0}\sqrt{1 + \frac{j\rho_0\omega N_p\Lambda'^2}{16\eta}}\right)^{-1}\right]^{-1}, \tag{17b}$$

where η is the dynamic viscosity of saturating air, γ is the ratio of the specific heat capacities, P_0 is atmospheric pressure, and N_p is the Prandtl number. Under the condition of 1 atmosphere and 20 °C in air, we choose $\eta \approx 1.8 \times 10^{-5}$Pa•s , $\gamma \approx 1.4$, $P_0 \approx 0.77$ and $N_p \approx 1.01325 \times 10^5$Pa . Doutres et al. measured and discussed the parameters associated to the JCA model of 15 polyurethane foams. According to the results of samples with low airflow resistivities, the values of five crucial parameters are set as shown in Table 2, where σ , α_∞ , ϕ , Λ and Λ' are static airflow resistivity, tortuosity factor, open porosity, viscous characteristic length and thermal characteristic length, respectively. Effective acoustic parameters can be obtained by substitute all the parameters into Eqs. 17(a) and (b).

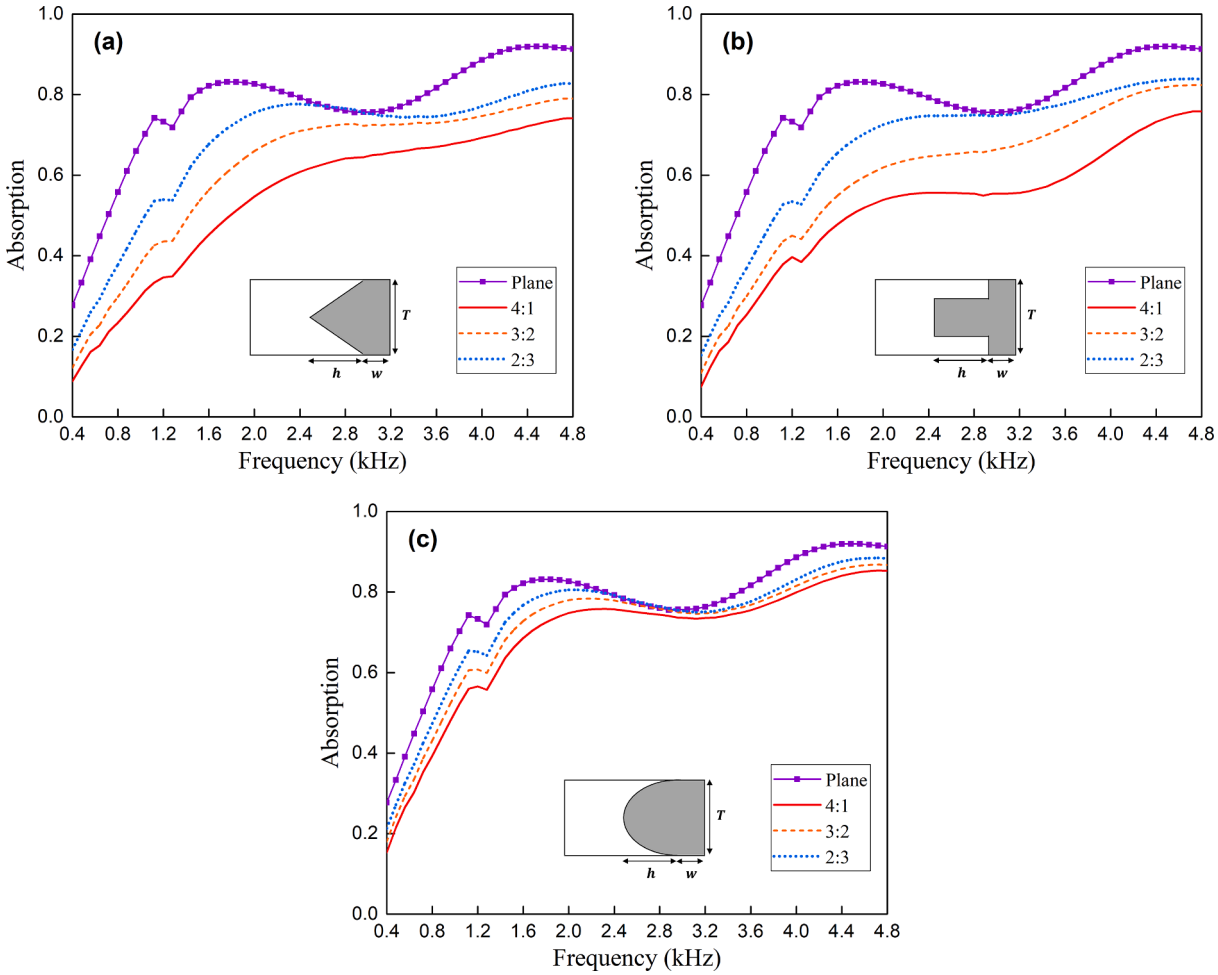

Fig. 10. Variations of absorption coefficients versus frequency for different h/w ratios and different surface shapes of (a) triangle, (b) rectangle, (c) ellipse.

Table 2
The parameters in JCA model.

$\sigma(N\bullet s/m^4)$	α_∞	$\phi(\%)$	$\Lambda(\mu m)$	$\Lambda'(\mu m)$
1000	1.06	98	400	600

5.2. *Effects of the shape*

The shape of the sound absorber influences the surface impedance of the structure, and then affects the sound absorption performance. Structures with different surfaces of plane, triangle, rectangle and ellipse in Fig. 7 with a constant overall thickness of 1 m are discussed here. The base thickness and structure period are randomly selected as $w = 30$cm and $T = 30$cm . The absorption coefficients of structures with different shapes predicted by the LRCWA method are shown in Fig. 11, and simulated results using FEM are also presented as verifications. The consistent results show that the absorption coefficients of structures with different shapes are very different in the frequency range from 60 Hz to 400 Hz. The sound absorption coefficient is not directly proportional to the material volume, and the plane structure with the largest material volume no longer have an absolute advantage in sound absorption performance. On the contrary, a proper shape can effectively improve the sound absorption coefficient.

5.3. *Effects of the geometric parameters*

In the design of sound absorber, besides the shape, the geometric parameters of the structure also need to be elaborately designed and optimized. A study of the structure with triangular surface is carried out as an example to show the effects of the geometric

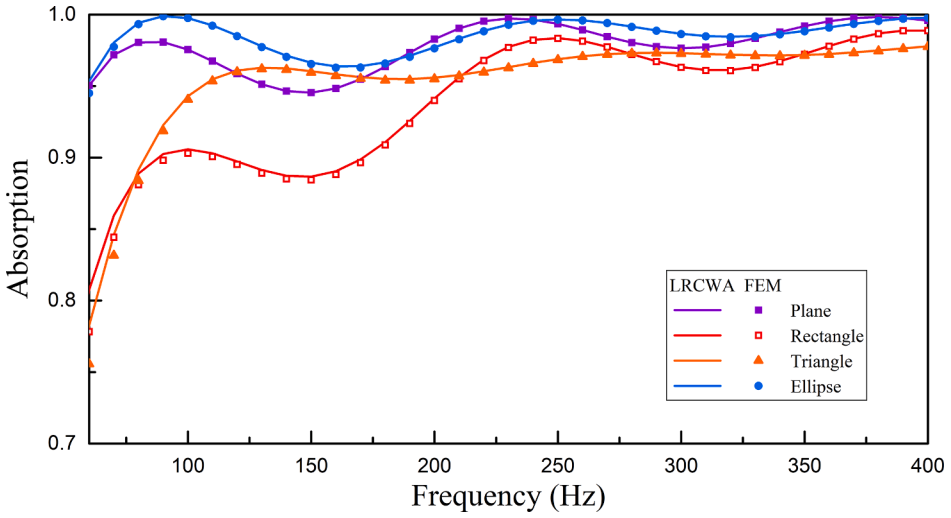

Fig. 11. Absorption coefficients in frequency range from 60 Hz to 400 Hz for structures with different surface shapes, whose base thickness and period are $w = 30\text{cm}$ and $T = 30\text{cm}$.

parameters on absorption performance. The studied geometric parameters include the base thickness w , structure period T and air gap thickness t_a . Usually, leaving an air gap between the sound absorber and the rigid wall will improve the sound absorption coefficient, so the air gap thickness is also considered in the discussion of the geometric parameters.

The base thickness of the triangular surface absorber with a constant period $T = 30\text{cm}$ and no air gap is investigated in six different values, from 10 cm to 1 m. Since the total thickness is fixed, as the base becomes thicker, its tip becomes thinner. The absorption coefficients for the triangular surface absorber with six different base thicknesses are shown in Fig. 12. When the base thickness is small, the absorption coefficient demonstrates a significant improvement by increasing the base thickness. When the base thickness increases to a certain value, the sound absorption coefficient begins to oscillate unsteadily, which is caused by standing waves formed in the base.

The absorption coefficients of the triangular surface absorber with different structure periods are shown in Fig. 13. The structure period varies by six different values from 10 cm to 60 cm, with a constant base thickness $w = 30\text{cm}$ and no air gap. Decreasing the structure period results in a sharper wedge. The results indicate that the absorption coefficient is almost not affected by the structure period. A similar situation exists in the predicted results for absorbers with surfaces of rectangle and ellipse.

The effect of the air gap thickness is investigated in six different values from 10 cm to 40 cm, with a constant base thickness $w = 30\text{cm}$ and a constant period $T = 30\text{cm}$. The air gap thickness is a safety margin and is not part of the overall thickness. According to the results shown in Fig. 14, the air gap behind the absorber has a great influence on the absorption coefficient.

5.4. Optimization of the absorber

From above discussion, both the shape and geometric parameters of the absorber will influence the sound absorption performance. In order to achieve high absorption in low frequency range, it is necessary to find the most appropriate surface shape and the optimal values of geometric parameters.

The method of LRCWA can predict the absorption coefficients of nonplanar periodic structures quickly and accurately. Using this semi-analytic method, the geometric parameters of the structure with triangular surface are scanned to obtain all its sound absorption coefficients, so as to select the geometric parameters with the best performance. The scanning range of the base thickness is 0–50 cm, and that of the air thickness is 0–50 cm. The structure period is not scanned but set as $T = 30\text{cm}$, because it has little effect on sound absorption. The evaluation standard is to maximize the minimum value of sound absorption coefficient in the frequency range of 60–400 Hz. According to the predicted results by LRCWA method, the optimal base thickness and air gap thickness are $w = 46.8\text{cm}$ and $t_a = 25.0\text{cm}$, respectively. The optimized structure with triangular surface is presented in Fig. 15(a), and the corresponding sound absorption coefficient is greater than 0.96 in the considered frequency range.

In addition to the conventional shape, we design a normalized surface shape formed by the superposition of five Gaussian functions that expressed as $y = \sum_{i=1}^{5} a_i e^{-(x-b_i)^2/2c_i^2}$, $(-2.5 \ll x \ll 2.5)$. The method of LRCWA is combined with genetic algorithm [30] to optimize the 15 parameters (a_i , b_i and c_i) affecting the surface shape and the air gap thickness t_a . The optimization range of parameters a_i and c_i is 0–1, that of parameter b_i is $-$ 2 to 2, and the range of air gap thickness is 0–50 cm. The optimization target is that the sound absorption coefficient is greater than 0.97 in the frequency range from 60 Hz to 400 Hz. The results of the 15 parameters optimized by genetic algorithm are shown in Table 3 and the optimal value of air gap thickness is 25.5 cm. The optimized structure formed by the superposition of Gaussian functions is shown in Fig. 15(b).

The optimized sound absorption coefficients in the considered frequency range are presented in Fig. 16, including those of the

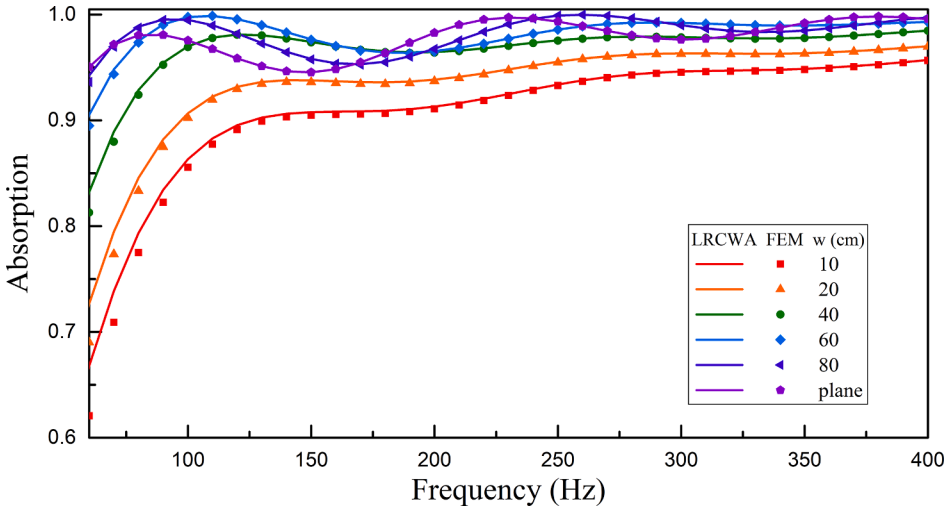

Fig. 12. Absorption coefficients of the triangular surface absorber with different base thicknesses w , whose period is fixed at $T = 30$cm without air gap.

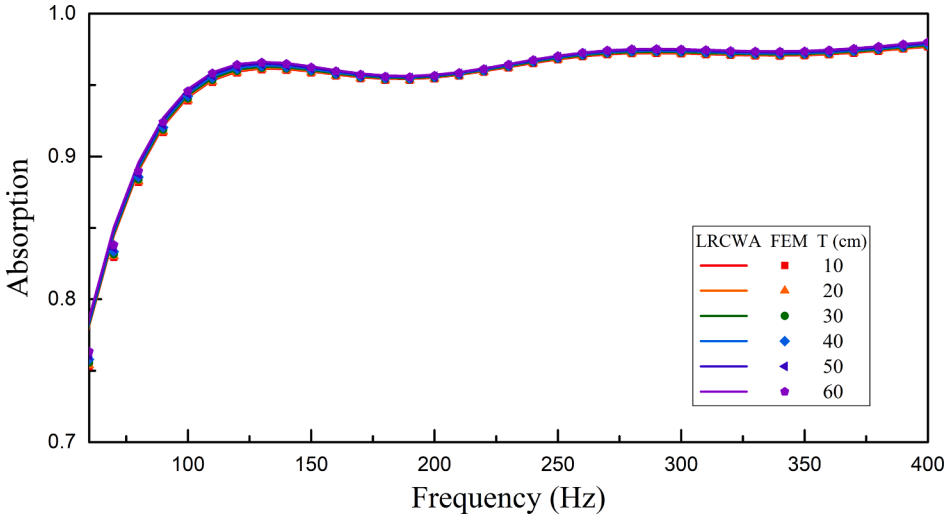

Fig. 13. Absorption coefficients of the triangular surface absorber with different structure periods T , whose base thickness is fixed at $w = 30$cm without air gap.

optimal structure with triangular surface and with Gaussian superposition surface. The absorption coefficient of the planar structure with a fixed thickness of 1 m is calculated for comparison, whose air gap thickness is the same as that of structure with triangular surface, i.e., 25.0 cm. The structures with nonplanar surfaces show better sound absorption performance than the planar structure in low frequency band. All absorption coefficients are also checked by simulation of FEM, and the results are consistent with the prediction by the LRCWA method.

6. Conclusions

In summary, we proposed a semi-analytic method of LRCWA that enables accurate predictions of absorption coefficients of nonplanar periodic structures. Firstly, the effective acoustic parameters of the porous material are quickly extracted by testing two flat structures with different thicknesses in the impedance tube system. Next, the structures with nonplanar surfaces are divided into several thin layers with approximately rectangular periodic modulation. Then, according to the periodic modulation of each layer, the coupling equations within the layers are obtained by expanding the sound pressures and quantities related to effective parameters into series form. Finally, the fundamental governing equations of the whole structure is established by connecting the interlayer boundary continuity conditions. Using the method of LRCWA, this study addressed the absorption coefficients of nonplanar absorbing sponges with different surface shapes. The applicability of the LRCWA method was verified by comparing with the experimental data and was

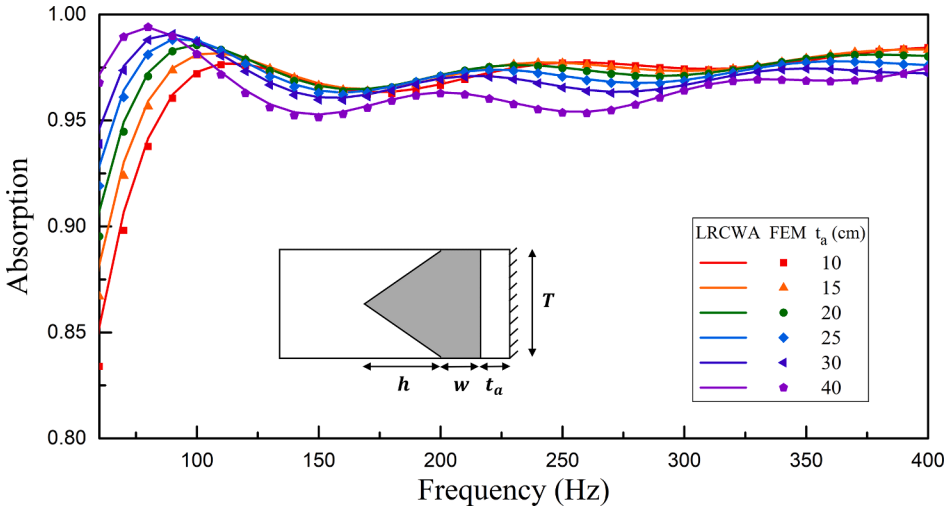

Fig. 14. Absorption coefficients of the triangular surface absorber with different air gap thicknesses t_a , whose base thickness and period are fixed at $w = 30\text{cm}$ and $T = 30\text{cm}$.

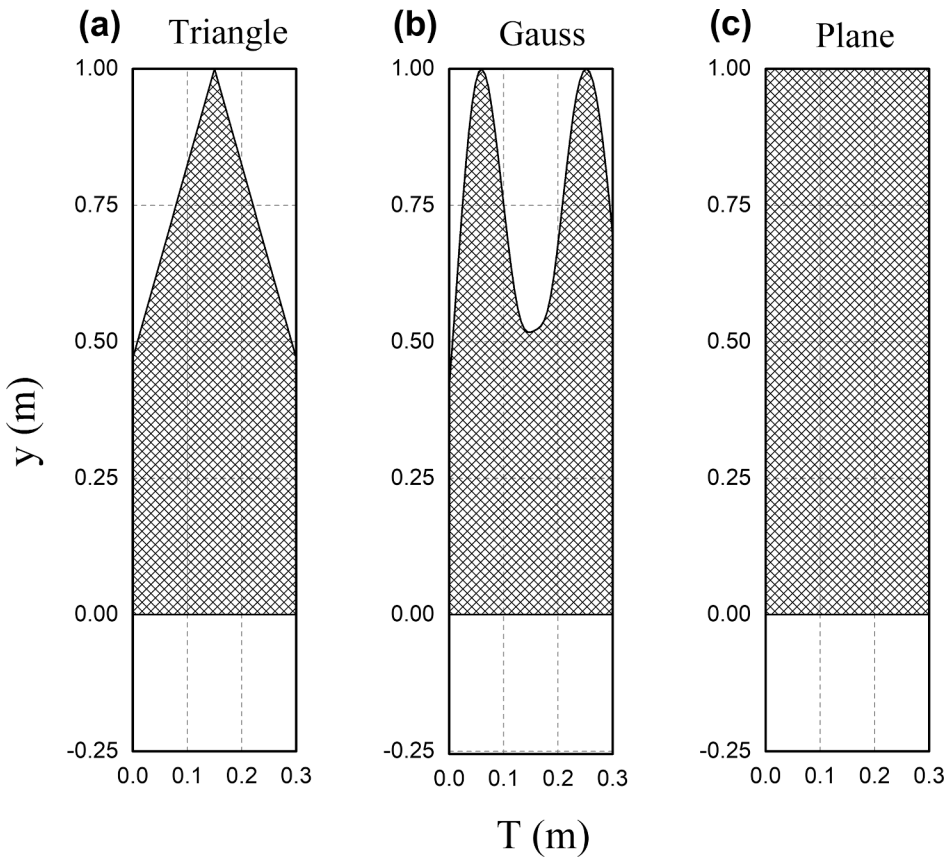

Fig. 15. Optimized structures with (a) triangular surface, (b) surface formed by the superposition of Gaussian functions and (c) the planar structure for comparison.

further validated by comparing with the simulation of FEM in a wide frequency range. The LRCWA method is applied to the design of sound absorber in low frequency range. The effects of surface shape and geometric parameters on sound absorption are discussed. And the geometric parameters of structure with triangular surface are scanned to obtain high sound abruption coefficients. Furthermore, combined with genetic algorithm, the surface formed by Gaussian function superposition is optimized to achieve good sound

Table 3
Optimal parameters of Gaussian superposition curve.

No.	1	2	3	4	5
a_i	0.3168	0.7706	0.0703	0.1242	0.4786
b_i	−1.2453	1.6993	0.1294	−0.4320	−1.7344
c_i	0.7335	0.9426	0.3073	0.5543	0.6673

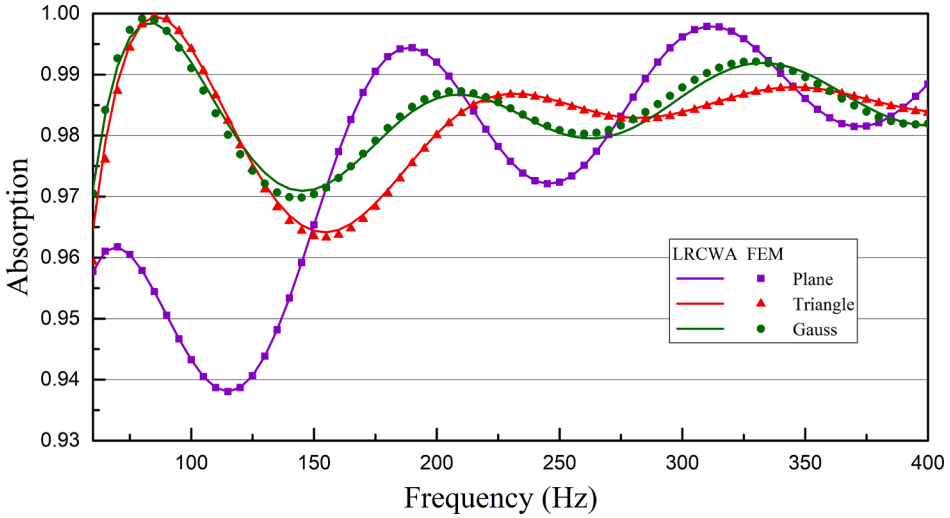

Fig. 16. Absorption coefficients of optimized structures with surface of triangle, Gaussian superposition, and that of the planar structure as a comparison.

absorption performance in a wide frequency band.

The LRCWA method is applicable to more complex structures even though only simple and usual shapes were discussed in this study. Besides the acoustic structures in the air, this method is also suitable for the calculation of underwater acoustic structures, which is important in the field of applied acoustics. The proposed semi-analytic method achieves a good balance between computational efficiency and applicability, and will be convenient to combine with optimization algorithms for delicate design and optimization. In addition, it does not need advanced periodic structure theory and tedious mathematical derivation, so it is easy to be implemented by other researchers and engineers.

CRediT authorship contribution statement

Yuzhen Yang: Conceptualizetion, Data curation, Formal analysis, Investigation, Methodology, Writing - original draft, Writing - review; **Han Jia:** Funding acquisition, Investigation, Project administration, Resource, Supervision, Writing - original draft, Writing - review; **Hailin Cao:** Funding acquisition, Project administration, Resource; **Xuecong Sun:** Data curation, Software; **Han Zhao:** Validation; **Yafeng Bi:** Investigation; **Jun Yang:** Funding acquisition, Project administration, Resource, Supervision.

Declaration of Competing Interest

The authors declare that they have no known competing financial interests or personal relationships that could have appeared to influence the work reported in this paper.

Acknowledgements

This work is supported by the Key-Area Research and Development Program of Guangdong Province (Grant No. 2020B010190002), and the National Natural Science Foundation of China (Grant No. 11874383, 12104480).

Data availability

The data that support the findings of this study are available from the corresponding author upon reasonable request.

References

[1] L.L. Beranek, H.P. Sleeper, The design and construction of anechoic sound chambers, J. Acoust. Soc. Am. 18 (1) (1946) 140–150.
[2] W. Koidan, G.R. Hruska, M.A. Pickett, Wedge Design for National Bureau of Standards Anechoic Chamber, J. Acoust. Soc. Am. 52 (4A) (1972) 1071–1076.
[3] I.V. Belyaev, A.Y. Golubev, A.Y. Zverev, S.Y. Makashov, V.V. Palchikovskiy, A.F. Sobolev, V.V. Chernykh, Experimental investigation of sound absorption of acoustic wedges for anechoic chambers, Acoust. Phys. 61 (5) (2015) 606–614.
[4] V. Easwaran, M.L. Munjal, Finite-element analysis of wedges used in anechoic chambers, J. Sound Vib. 160 (2) (1993) 333–350.
[5] C.-N. Wang, M.-K. Tang, Boundary element evaluation on the performance of sound absorbing wedges for anechoic chambers, Eng. Anal. Bound. Elem. 18 (2) (1996) 103–110.
[6] P. Bonfiglio, F. Pompoli, Numerical methodologies for optimizing and predicting the low frequency behavior of anechoic chambers, J. Acoust. Soc. Am. 134 (1) (2013) 285–291.
[7] C. Jiang, S. Zhang, L. Huang, On the acoustic wedge design and simulation of anechoic chamber, J. Sound Vib. 381 (2016) 139–155.
[8] M.E. Tavakkoli Nejad, A. Loghmani, S. Ziaei-Rad, The effects of wedge geometrical parameters and arrangement on the sound absorption coefficient – a numerical and experimental study, Appl. Acoust. 169 (2020), 107458.
[9] Y.J. Kang, J.S. Bolton, Optimal design of acoustical sponge treatments, J. Vibr. Acoust. 118 (3) (1996) 498–504.
[10] Y.J. Kang, J.S. Bolton, Sound transmission through elastic porous wedges and sponge layers having spatially graded properties, J. Acoust. Soc. Am. 102 (6) (1997) 3319–3332.
[11] W.-H. Chen, F.-C. Lee, D.-M. Chiang, On the acoustic absorption of porous materials with different surface shapes and perforated plates, J. Sound Vib. 237 (2) (2000) 337–355.
[12] F. Simón, R.M. Rodríguez, J. Pfretzschner, On the absorption coefficient of porous corrugated surfaces, J. Vibr. Acoust. 124 (3) (2002) 329–333.
[13] T. Kar, M.L. Munjal, Plane wave analysis of acoustic wedges using the boundary-condition-transfer algorithm, Appl. Acoust. 67 (9) (2006) 901–917.
[14] H.-S. Tsay, Analysis of normal incidence absorption of pyramidal polyurethane sponge by three-dimensional finite element frequency domain acoustical analysis, J. Acoust. Soc. Am. 120 (5) (2006) 2686–2693.
[15] J.-F. Allard, O. Dazel, G. Gautier, J.-P. Groby, W. Lauriks, Prediction of sound reflection by corrugated porous surfaces, J. Acoust. Soc. Am. 129 (4) (2011) 1696–1706.
[16] H.-S. Tsay, F.-H. Yeh, Optimal design of corrugated cellular plastic sponge with semi-elliptical shaped upper surface by finite element frequency domain acoustic analysis, J. Cell. Plast. 43 (3) (2016) 197–214.
[17] J. Zhao, Z. Chen, M. Bao, S. Sakamoto, Prediction of sound absorption coefficients of acoustic wedges using finite-difference time-domain analysis, Appl. Acoust. 155 (2019) 428–441.
[18] X. Yang, Y. Wang, H. Yu, Sound performance of multilayered composites, J. Mater. Manuf. Process. 22 (6) (2007) 721–725.
[19] D. Magliacano, M. Ouisse, S.D. Rosa, F. Franco, A. Khelif, Computation of acoustic properties and design guidelines of periodic Biot-modeled foams, Appl. Acoust. 168 (2020), 107428.
[20] D. Magliacano, G. Petrone, F. Franco, S. De Rosa, Numerical investigations about the sound transmission loss of a fuselage panel section with embedded periodic foams, Appl. Acoust. 182 (2021), 108265.
[21] Y. Yang, H. Jia, J. Yang, Study on asymmetric diffraction of acoustic parity-time-symmetric gratings using rigorous coupled-wave analysis, J. Acoust. Soc. Am. 148 (1) (2020) 33–43.
[22] K. Knop, Rigorous diffraction theory for transmission phase gratings with deep rectangular grooves, J. Opt. Soc. Am. 68 (9) (1978) 1206–1210.
[23] M.G. Moharam, T.K. Gaylord, Rigorous coupled-wave analysis of planar-grating diffraction, J. Opt. Soc. Am. 71 (7) (1981) 811–818.
[24] Z. Zylberberg, E. Marom, Rigorous coupled-wave analysis of pure reflection gratings, J. Opt. Soc. Am. 73 (3) (1983) 392–398.
[25] M.G. Moharam, T.K. Gaylord, Rigorous coupled-wave analysis of metallic surface-relief gratings, J. Opt. Soc. Am. A 3 (11) (1986) 1780–1787.
[26] N. Chateau, J.P. Hugonin, Algorithm for the rigorous coupled-wave analysis of grating diffraction, J. Opt. Soc. Am. A 11 (4) (1994) 1321–1331.
[27] M.G. Moharam, E.B. Grann, D.A. Pommet, T.K. Gaylord, Formulation for stable and efficient implementation of the rigorous coupled-wave analysis of binary gratings, J. Opt. Soc. Am. A 12 (5) (1995) 1068–1076.
[28] T.J. Cox, P. D'Antonio, Acoustic absorbers and diffusers: theory, design and application, 3rd ed., CRC Press, Boca Raton, 2017, p. 206.
[29] O. Doutres, N. Atalla, K. Dong, Effect of the microstructure closed pore content on the acoustic behavior of polyurethane foams, J. Appl. Phys. 110 (6) (2011) 064901.
[30] Y.-C. Chang, L.-J. Yeh, M.-C. Chiu, Optimization of double-layer absorbers on constrained sound absorption system by using genetic algorithm, Int. J. Numer. Meth. Eng. 62 (3) (2005) 317–333.